

MICROSTRUCTURAL DISTRIBUTIONS IN EXTRUSION BLOW MOLDED SEMICRYSTALLINE RESINS

Alan H. Wagner*, Dilhan M. Kalyon, and Victor Tan**
Highly Filled Materials Institute
Stevens Institute of Technology
Hoboken, NJ 07030

* Currently with Cytec Industries, Stamford CT

** Polymer Processing Institute at Stevens Institute of Technology

Introduction

As applications for blow molded parts become more demanding, resins are being pushed to their limits to satisfy various ultimate performance criteria at minimum thickness. However, minimizing the wall thickness of a blow molded bottle while still maintaining a high level of performance requires a detailed understanding of the development of microstructural distributions. A highly oriented and crystallized resin will exhibit very different physical, clarity and barrier properties than the same resin with a higher amorphous content. Specifically, the rate of cooling distributions affect the final part crystallinity distribution since the crystallization kinetics of most polymers are temperature dependent. The incorporation of a fibrous filler or impact modifier can also have a profound effect on microstructural distributions and the resulting ultimate properties of a molded part.

Early work using empirical correlations to link various properties (haze, impact resistance shrinkage, etc.) to operating conditions met with limited success [1-6]. Kamal and Kalyon [7-9] reported on the effects of cooling rate, contact temperature, and part thickness on part crystallinity, orientation, and density profiles. White et. al. [10,11] utilizing x-ray scattering and pole figures presented orientation distributions for blow molded polyethylene and PET bottles. Recently, numerical predictions of crystallinity distributions, residual stresses and part shrinkage have been presented [12-14].

In the current study, the crystallinity, thickness, density, and birefringence distributions, and fiber orientation of blow molded bottles of neat and glass fiber filled resins and ultimate properties of blown bottles were characterized.

Materials

Two high density polyethylene resins (HDPE) and two polyamide resins were used. One HDPE, PE1, was

produced via a chromium catalyst while the second HDPE, PE3, was produced via the Ziegler-Natta type reaction. The first polyamide, PA1, is a chain extended, multi-branched, natural colored polyamide 6. The second polyamide resin, PA2, is a chain extended, multi-branched polyamide 6 containing 12% (by weight) chopped glass fibers and carbon black. Polyamide is a relative new comer to the blow molding industry due to its traditionally low viscosity at processing temperatures. Recent developments in the manufacturing of polyamide have allowed the resin to possess greater melt strength and higher viscosity via chain extenders, branching, blending, and filling.

Experimental

A Krupp-Kautex, model KEB2-14, continuous extrusion blow molding machine was employed in this study. The blow molding machine was equipped with a convergent / divergent bushing and pin system. A standard commercial cylindrical mold which produced a bottle 65 mm in diameter and 200 mm high was utilized.

The top and bottom of each bottle was removed and the resulting cylinder was slit vertically 90° from the parting line to produce a flat sheet. A 10 x 10 mm grid was superimposed on the sheet of plastic and the thickness was measured at each grid intersection with a resolution of 0.001 mm.

The crystal content was directly determined from DSC latent heat of fusion measurements. The weight fraction of the crystalline phase, X_c , as given by heat of fusion measurements is:

$$X_c = \frac{(\Delta H_f)}{(\Delta H_f^0)} \quad (1)$$

where ΔH_f and ΔH_f^0 are the values of the heat of fusion for the sample and the pure crystalline material,

respectively. The heat of fusion for single crystals of polyamide-6 and HDPE are 230 J/g and 293 J/g, respectively. A Perkin Elmer differential scanning calorimeter, DSC-4, was used to gather the specific heat and heat of fusion data.

Three small (5 x 5 mm) squares were cut from the blow molded bottles at locations which were adjacent to the heat flux sensor located in the mold wall. One square was analyzed as cut to yield a bulk fraction crystallinity. The second square was microtomed from the outside surface to the inner surface at 20 μm intervals while the third square was microtomed from the inside surface to the outside surface. Each microtomed section was analyzed by DSC to yield a fraction crystallinity versus depth profile. The glass filled polyamide sample (PA2) was too hard to be sectioned with the microtome and was not analyzed with this technique.

The birefringence profile developed in polymer processing operations such as injection and blow molding is the result of two separate effects [15,16]. First, transient thermal gradients quench the skin layers while the core is cooled at a slower rate. This gives rise to compressive residual stresses at the skin and tensile stresses at the core and leads to anisotropy and hence to birefringence. The second mechanism involves the flow-induced orientation of the macromolecules during processing [17]. Upon orientation, the varying polarisabilities of the chains in different directions give rise to different velocities of light in different directions and therefore to different refractive indices. The difference of refractive indices along two orthogonal directions, Δn , is related to orientation distributions:

$$\Delta n = n_z - n_y = \frac{\Delta}{H} \quad (2)$$

where n_z and n_y are the refractive indices in the z (machine) and y (thickness) directions, respectively; Δ is the path difference measured with the compensator, and H is the thickness of the sample.

The birefringence measurements were performed on a Zeiss Universal Pol polarizing microscope. A Nikitin-Berek type compensator was used to determine the path difference in the sample.

Contact microradiography [18] was employed to study the structural features of the blown samples of glass filled polyamide. For contact microradiography, relatively soft x-ray white radiation was used. A GE GA5 x-ray unit with a copper target at 15 kV and 1 mA excitation was employed. Samples of the bottle wall with

frozen-in fiber orientation were reduced in thickness to 0.1 to 0.25 mm by grinding with progressively finer grit sizes of bonded abrasive paper, concluding with a polishing operation.

A Dew and Gumms double micro-tensile bar (ASTM Type 5) punch and a Herman Schwabe Inc, Model 288 die cutting press were used to cut samples out of the molded articles. The tensile bars were pulled on a Instron Universal Testing machine, model TTD, equipped with 2 inch spring clamps and a 200 pound load cell. The tensile bars were conditioned at 25 $^{\circ}\text{C}$ and 50% humidity for 24 hours prior to testing.

Results and Discussion

The typical three dimensional thickness map of a HDPE blow molded bottle is shown in Figure 1. The parting lines located at 5.5 and 15.5 cm. Following any circumferential position from top of the bottle to bottom of the bottle it is observed that the bottle wall is thinnest at the top and gets progressively thicker until reaching the bottom where it again decreases. The thickness also varies greatly in the circumferential direction. There is an increase in the thickness at the parting lines with a local minimum located between the two parting lines. On the other hand, the fiber filled polyamide produced a more uniform bottle, as shown in Figure 2, in comparison to the high density polyethylene resins. Except for the thinning near the top and bottom of the bottle, the bottle wall thickness is uniform in the axial direction. The circumferential thickness distribution exhibits the typical thickening at the parting lines [9].

As the wall thickness increases, the time needed for cooling during solidification also increases. The extra time available to the thicker walled portion of a bottle will manifest itself as an increase in crystallinity. Figures 3 and 4 represent the density distributions of HDPE and polyamide resins, respectively. Due to the much faster crystallization/nucleation rate of polyamide as well as the lower equilibrium fraction crystalline phase of polyamide, the polyamide resin achieves a constant crystallinity content which does not change from location to location. However, the degree of crystallinity distributions of HDPE indicate sensitivity of the rate of crystallization of HDPE to temperature history (Figure 5). The comparison of the fraction crystallinity distribution for the two polyethylenes reveals that PE1 exhibits greater crystallinity than PE3 at similar thickness. Analysis of rates of crystallization of these two resins reveals that PE1 indeed crystallizes at a faster rate than PE3.

The distribution of crystallinity between the outside and inside surfaces of the blow molded bottles are shown in Figure 6. The crystallinity of HDPE increases linearly from a minimum value of 63% near the outer

surface to 70% crystalline at the inner surface of the bottle. Neat polyamide on the other hand exhibits a more uniform crystallinity profile which increases slowly from 25% at the outside to 30% at the inside surface of the bottles.

When the inflating polymer first touches the cold mold wall, a layer of polymer will immediately freeze at the surface retaining the orientation arising from the previous orientation history. As one progresses from the parison / mold interface towards the inside of the bottle more time is available for relaxation before solidification. As shown in Figure 7, birefringence or optical anisotropy generally decreases from a maximum near the outer surface to a minimum at or near the inner surface of the blow molded article.

Although substantial differences in thickness and hence cooling rates exist, there were no statistically significant differences in ultimate tensile properties from location to location for the unfilled resins (PE1, PE3, and PA1). Furthermore, bottles composed of the glass filled polyamide did exhibit significant differences in tensile strength at yield along the machine direction and perpendicular to the machine direction. Microradiographs of the bottle wall revealed that the fibers were oriented along the long axis of the bottle, ie. In the machine direction (Figure 8), giving rise to the greater yield stress measured along the machine direction.

Acknowledgments

The authors would like to acknowledge the contributions of Drs. Paul Tong and Pradeep Shirodkar of Mobil Chemical Company and Messrs. Dan Leydon and Tom Krolick of Allied-Signal Corporation, as well as the financial support of Mobil Chemical Company and Allied-Signal Corporation. The microradiography was carried out by Dr. R. Yazici of HFMI, and some of the crystallinity measurements were carried out by Mr Suwardi and Ms. Boz of HFMI and Dr. P. Tong of Mobil.

References

1. H. Frank and W. Wengler, *Verpack Rundt*, **22**, 10, 1382 (1971).
2. M. Dixon, *Plast. Inst. Trans. J.*, **13** (1963).
3. J. Terenzi, R. Griffith and C. Deeley, *SPE ANTEC Tech. Pap.*, 745 (1967).
4. W. Daubenbechel, *Kunststoffe*, **66**, 7 (1976).
5. W. Kendall, *Plast. Inst. Trans. J.*, **49** (1963).
6. S. Harata, and A. Kishimoto, *Polym. Eng. Sci.*, **10**, 4, 235 (1970).
7. M. R. Kamal, V. Tan, and D. M. Kalyon, *Polym. Eng. Sci.*, **21**,6,331 (1981).
8. M, R, Kamal, D. M. Kalyon and V. Tan, *Polym. Eng. Sci.*, **22**, 5, 287 (1982).
9. M. R. Kamal and D. M. Kalyon, *Polym. Eng. Sci.*, **23**, 9, 503 (1983).
10. M. Cakmak, J. E. Spruiell, and J. L. White, *Polym. Eng. Sci.*, **24**, 18, 1390 (1984).
11. K. J. Choi, J. E. Spruiell, and J. L. White, *Polym. Eng. Sci.*, **29**, 7, 463 (1989).
12. J. S. Yu and D. M. Kalyon, *Plas. And Rub. Proc. And Appl.*, **15**, 1 (1991).
13. R. W. DiRaddo and A. Garcia-Rejon, *SPE ANTEC Tech. Pap.*, 1042 (1994).
14. D. Laroche, J. F. Hetu, L. Pecora, R. W. DiRaddo, M. Grenier, and D. Brougham, *SPE ANTEC Tech. Pap.*, 919 (1995).
15. J. Saffell and A. Windle, *J. Appl. Polym. Sci.*, **25**, 1117 (1980).
16. C. Wust and D. Bogue, *J. Appl. Polym. Sci.*, **28**, 1931 (1983).
17. H. Heron, S. Pedersen, and L. Chapoy, *Rheol. Acta.*, **15**, 379 (1976).
18. A. Green, Ed. Handbook of Nondestructive Inspection and Quality Control, ASM, 2 9 5 (1990).

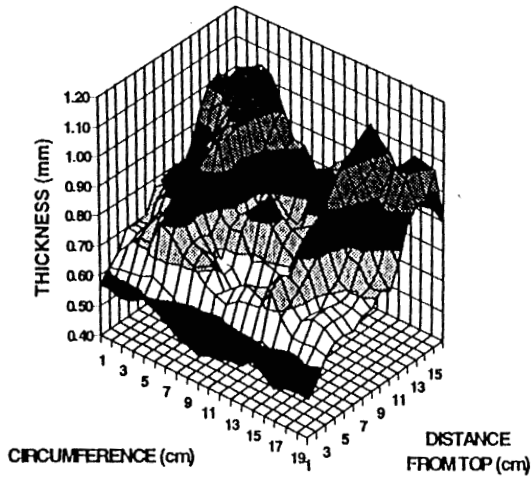


Figure 1, Bottle Wall Thickness Distribution for HDPE, PE1

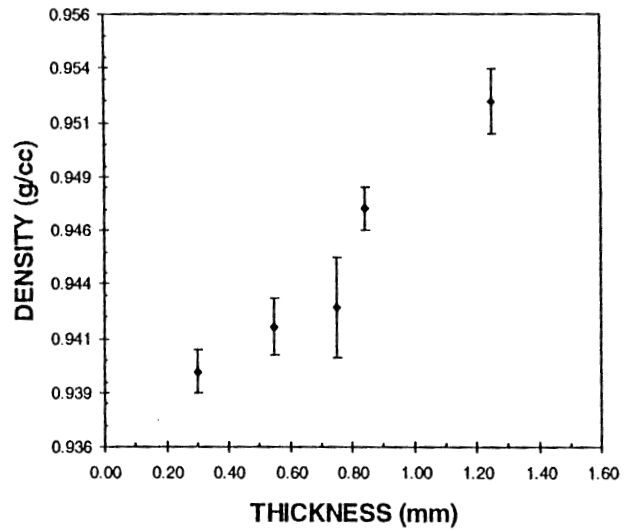


Figure 3, Effect of Bottle Wall Thickness on Density for HDPE (PE1)

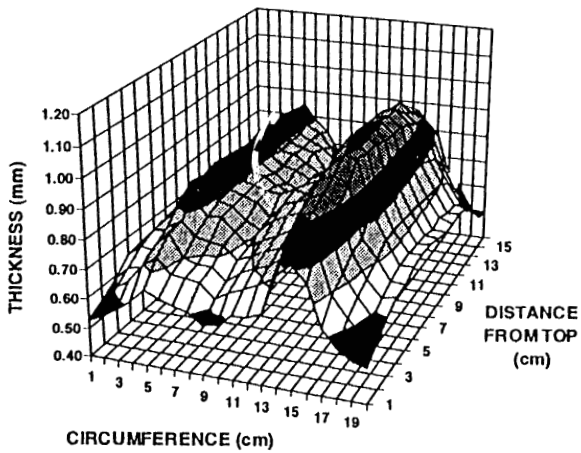


Figure 2, Bottle Wall Thickness Distribution for Glass Fiber Filled Polyamide (PA2)

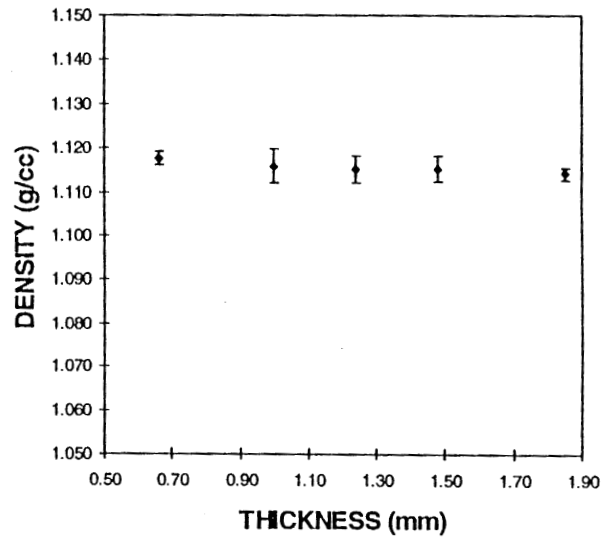


Figure 4, Effect of Bottle Wall Thickness on Density for Neat Polyamide (PA1)

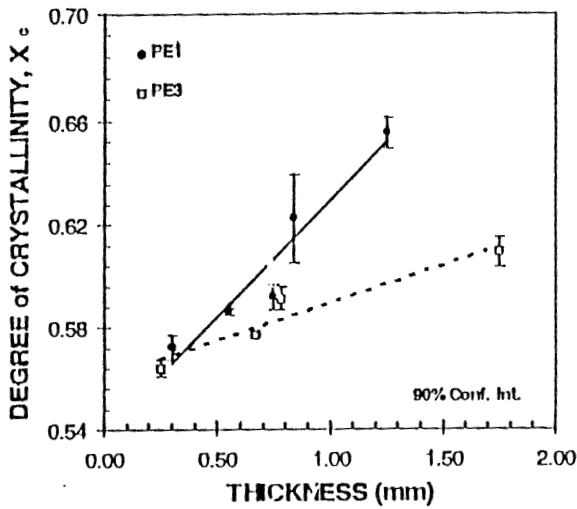


Figure 5, Effect of Crystallization Rate on Degree of Crystallinity for HDPE

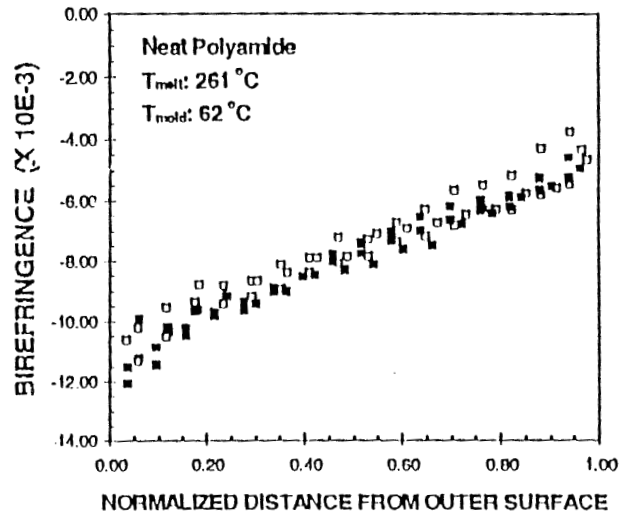


Figure 7, Birefringence Distribution of Neat Polyamide (PA1)

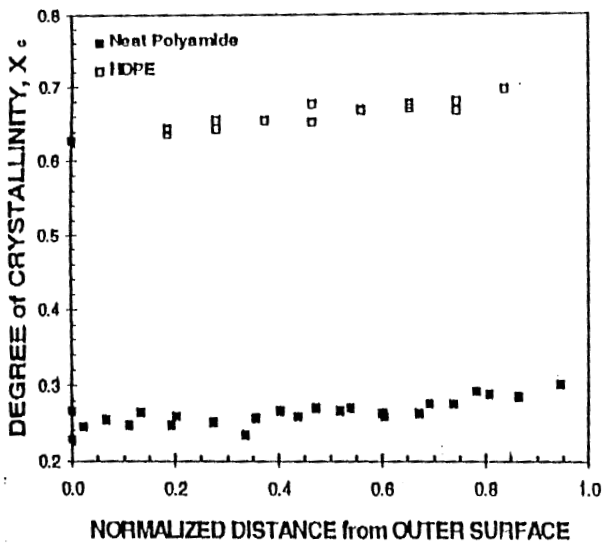


Figure 6, Degree of Crystallinity Versus Distance from the Outside Surface for HDPE (PE1) and Neat Polyamide (PA1)

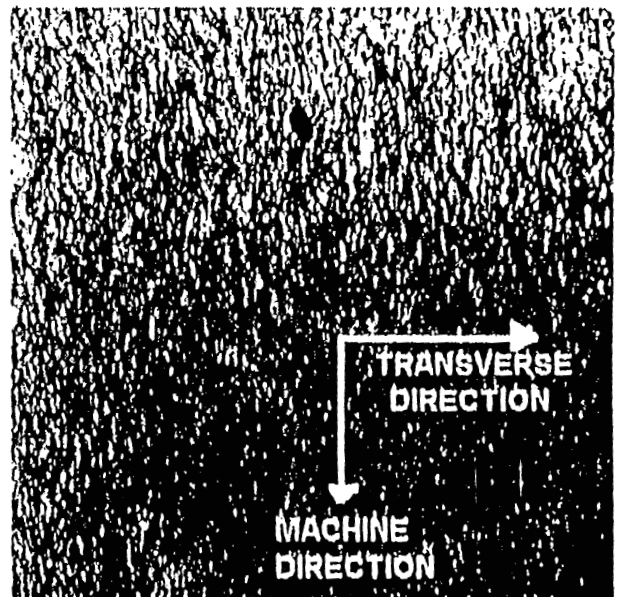


Figure 8, Fiber Orientation in the Bottle Wall for Fiber Reinforced Polyamide (PA2)